

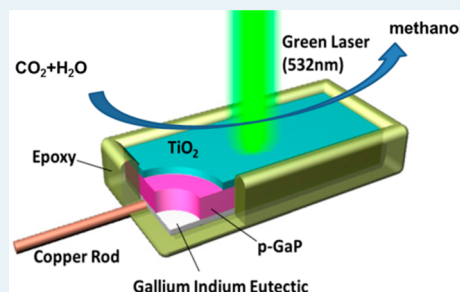
CO₂ Reduction to Methanol on TiO₂-Passivated GaP PhotocatalystsGuangtong Zeng,[†] Jing Qiu,[‡] Zhen Li,[§] Prathamesh Pavaskar,[§] and Stephen B. Cronin^{*,†,§}[†]Department of Chemistry, [‡]Department of Materials Science, and [§]Department of Electrical Engineering, University of Southern California, Los Angeles, California 90089, United States

Supporting Information

ABSTRACT: In the past, the electrochemical instability of III–V semiconductors has severely limited their applicability in photocatalysis. As a result, a vast majority of the research on photocatalysis has been done on TiO₂, which is chemically robust over a wide range of pH. However, TiO₂ has a wide band gap (3.2 eV) and can only absorb ~4% of the solar spectrum, and thus, it will never provide efficient solar energy conversion/storage on its own. Here, we report photocatalytic CO₂ reduction with water to produce methanol using TiO₂-passivated GaP photocathodes under 532 nm wavelength illumination. The TiO₂ layer prevents corrosion of the GaP, as evidenced by atomic force microscopy and photoelectrochemical measurements. Here, the GaP surface is passivated using a thin film of TiO₂ deposited by atomic layer deposition (ALD), which provides a viable, stable photocatalyst without sacrificing photocatalytic efficiency.

In addition to providing a stable photocatalytic surface, the TiO₂ passivation provides substantial enhancement in the photoconversion efficiency through passivation of surface states, which cause nonradiative carrier recombination. In addition to passivation effects, the TiO₂ deposited by ALD is n-type due to oxygen vacancies and forms a pn-junction with the underlying p-type GaP photocathode. This creates a built-in field that assists in the separation of photogenerated electron–hole pairs, further reducing recombination. This reduction in the surface recombination velocity (SRV) corresponds to a shift in the overpotential of almost 0.5 V. No enhancement is observed for TiO₂ thicknesses above 10 nm, due to the insulating nature of the TiO₂, which eventually outweighs the benefits of passivation.

KEYWORDS: photoelectrochemical, GaP, CO₂ reduction, TiO₂ passivated, methanol



The photoelectrochemical reduction of CO₂ is an exciting reaction system with the ability to convert an abundant greenhouse gas to combustible hydrocarbon fuels using sunlight. The direct conversion of solar-to-chemical energy has several advantages over solar-to-electric energy conversion, most notably, the ability to store large amounts of energy (~GW) in chemical bonds that can later be released in a carbon neutral cycle.¹ Many attempts have been made to reduce CO₂ by 2e⁻ to various species such as CO and formic acid, as reported in previous literature.² Few researchers have achieved further reduction to CH₃OH or CH₄.³ Methanol is an attractive product with a relatively high energy density, which can be easily integrated into the existing liquid fuel technologies.^{1g,4} However, the photocatalytic reduction of CO₂ with H₂O to methanol requires six electrons and many intermediate species, some of which have extremely high energy barriers.⁵ The most likely first step in this multielectron reaction is the one electron reduction to the CO₂⁻ intermediate,⁶ which lies 1.7 eV above the conduction band of TiO₂ and 1.2 eV above GaP. The mechanism for electrochemical CO₂ reduction was first proposed by Bockris et al.⁷ The high overpotential required for this reaction was attributed to the formation of the CO₂⁻ intermediate, which consequently converts to CO via the general process CO₂ + e⁻ → CO₂⁻, CO₂⁻ + 2H⁺ + e⁻ → CO + H₂O.^{1c,i,3a,8} In 1978, Hallman's group first reported CO₂ reduction on p-GaP under 365 nm illumination with an applied overpotential of -1.4 V (vs SCE).^{2a} Fujishima and

Honda demonstrated photoelectrocatalytic reduction of CO₂ to formaldehyde and methanol by irradiating TiO₂ and GaP with the UV light at an overpotential of -1.5 V (vs SCE).^{2b,9} Canfield later reported CO₂ reduction to methanol on p-InP with an overpotential of -1.3 V (vs SCE).^{2h} More recently, Bocarsly's group demonstrated pyridinium-catalyzed CO₂ reduction on GaP photocathodes with overpotentials between -0.7 V and -0.2 V (vs SCE) under UV light.^{3a} Despite these interesting prior results, the stability of these materials against photocorrosion has not been addressed.

In the work presented here, we investigate the photocatalytic performance and stability of TiO₂-passivated p-GaP using atomic force microscopy (AFM), photoelectrochemistry, and optical microscopy. The photocatalytic efficiency is studied systematically as a function of TiO₂ layer thickness using a three-terminal potentiostat. The products are detected using NMR spectroscopy and gas chromatography, systematically as a function of applied overpotential.

Zn doped p-type (100) oriented GaP with a dopant concentration of 2 × 10¹⁸ cm⁻³ was used as the photocatalyst for CO₂ reduction with an active area of 0.5 cm × 1 cm. Atomic layer deposition (ALD) of anatase TiO₂ was performed at 250 °C on the p-GaP wafers with TiCl₄ as the titanium source and

Received: March 11, 2014

Revised: August 21, 2014

Published: September 3, 2014

water vapor as the oxygen source. The antase crystal phase was verified by Raman spectroscopy. Using ellipsometry, we established that 100 cycles of ALD produces a 4 nm thick TiO₂ film and 1000 cycles produces a 40 nm film. A Ga–In eutectic film was painted on the back of the p-GaP to form an Ohmic contact. The Ga–In contact was then connected to the external circuitry with a copper wire and coated with epoxy cement to insulate it from the electrolytic solution, as illustrated in Figure 1b. Although this planar geometry is not ideal for high

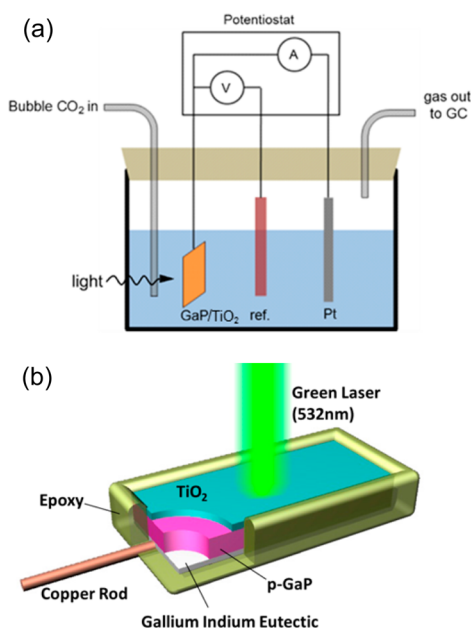


Figure 1. Schematic diagram of (a) photoelectrochemical measurement setup and (b) sample geometry of the TiO₂-passivated p-GaP photocathode.

efficiency photoconversion, it enables us to study surface stability. A three-terminal potentiostat was used with the prepared semiconductor samples as the working electrode, a Ag/AgCl electrode as the reference electrode, and a Pt electrode functioning as a counter electrode, as shown in Figure 1a. The photocatalytic reaction rates of two sets of samples were measured in a 2 mL solution of 0.5 M NaCl, with and without 10 mM pyridine, while continuously bubbling CO₂ through the solution. NaCl (0.5 M) was chosen as the electrolyte solution because of its high conductance and its ability to stabilize the intermediate states involved in the CO₂ reduction.¹⁰ In this setup, we analyze the products evolving at the working electrode, instead of at the counter electrode. It is likely that oxygen is also produced in the reaction.

While photocatalysis on GaP (and other III–V compound semiconductors) has been demonstrated previously,^{2h,3a,11} this material corrodes rapidly under photoelectrochemical conditions and is significantly degraded after just 30 min of illumination. In order to make GaP photochemically stable, we passivated the surface using a thin film of TiO₂ deposited by ALD, as illustrated schematically in Figure 1b. Figure 2a,b show optical microscope and atomic force microscope images of the bare GaP surface after 8 h of illumination. Figure 2c shows a plot of the surface topography obtained along the dashed white line in Figure 2b, showing an RMS roughness of ± 54 nm, which indicates that substantial photocorrosion has taken place and that this will not serve as a viable photocatalyst. In contrast,

the photocurrent density of TiO₂-passivated GaP is stable for 8 h. The optical microscope image (Figure 2d) and atomic force microscope image (Figure 2e) exhibit no evidence of surface corrosion or damage after 8 h, with an RMS roughness of ± 1 nm (Figure 2f), indicating that this is a long-term, stable photocatalyst. Here, the TiO₂ significantly improves the photostability of the GaP surface, however, more extensive time-dependent studies are needed in order to establish the extent of this long-term stability.

In addition to providing a stable photocatalytic surface, the TiO₂ passivation layer results in an increase in the photoconversion efficiency. Figure 3a shows the photocurrent–voltage curves for GaP passivated with various thicknesses of TiO₂ measured in a 0.5 M NaCl, 10 mM pyridine solution under 532 nm illumination. During these measurements, CO₂ is continuously bubbled through the solution. Bare GaP (green curve) has an onset of photocurrent at a potential of approximately -0.15 V (vs NHE). For TiO₂-passivated GaP, we see a clear shift in the overpotential required to drive this reaction with increasing thickness of the TiO₂, as plotted in Figure 3b. Table 1 lists the shift of onset overpotential of samples with different thicknesses of TiO₂. For example, the onset potential for 10 nm TiO₂ (red curve) is shifted by 0.5 V with respect to bare GaP. This shift is attributed to the passivation of surface states that cause nonradiative recombination and the formation of a pn-junction, which is created because the ALD-deposited TiO₂ tends to be n-type doped due to oxygen vacancies.¹² Figure 3c shows the built-in potential for the junction calculated using $V_{bi} = \left(\frac{(W_D q)}{2 \epsilon_0 \epsilon_a \epsilon_d} \right) \left(\frac{N_a N_d (\epsilon_a + \epsilon_d)}{(N_a + N_d)^2} \right)$, assuming a doping concentration of $N_a = 5 \times 10^{18} \text{ cm}^{-3}$.¹³ Here, W_D is the depletion width of the GaP–TiO₂ junction, which is a function of the TiO₂ layer thickness. This simple calculation predicts values similar to the experimentally observed shift in the overpotential plotted in Figure 3b. Beyond 10 nm, however, the photocurrent decreases rapidly with increasing TiO₂ thickness due to band bending at the n-type TiO₂/electrolyte interface, which blocks electrons. No enhancement is observed for TiO₂ thicknesses above 10 nm, due to the insulating nature of the TiO₂, which eventually outweighs the benefits of passivation. Although TiO₂ does not absorb light at 532 nm, the pn-junction formed with the GaP enables separation of the photogenerated charge in the actively absorbing GaP. Figure 3d shows the NMR spectra taken after 8 h of illumination with an overpotential of -0.50 V vs NHE for GaP with and without TiO₂ passivation. These data show a clear peak corresponding to methanol, as reported previously by Barton et al.^{3a} Gas chromatography FID data have also been used to verify the production of methanol, as shown in Supporting Information Figure S1. On the basis of these GC FID data for the 5 nm thick TiO₂ sample, we calculated that $4.9 (\pm 0.02) \mu\text{mol}$ of CH₃OH are produced during an 8 h reaction consuming 5.2 Coulombs of charge. Dividing by this ratio by the stoichiometric factor of 6, yields a Faradaic efficiency of 55%. Also, according to the GC TCD data of the same experiment, H₂ is produced with a Faradaic efficiency of 30%. The photoconversion efficiency, however, can be significantly less than this due to nonradiative recombination, which is unknown, particularly for this planar sample geometry. As a control experiment, the same reaction was run under the same electrochemical conditions of -0.50 V vs NHE without laser illumination, which resulted in no measurable current and no detectable methanol in the NMR spectra. In order to rule out

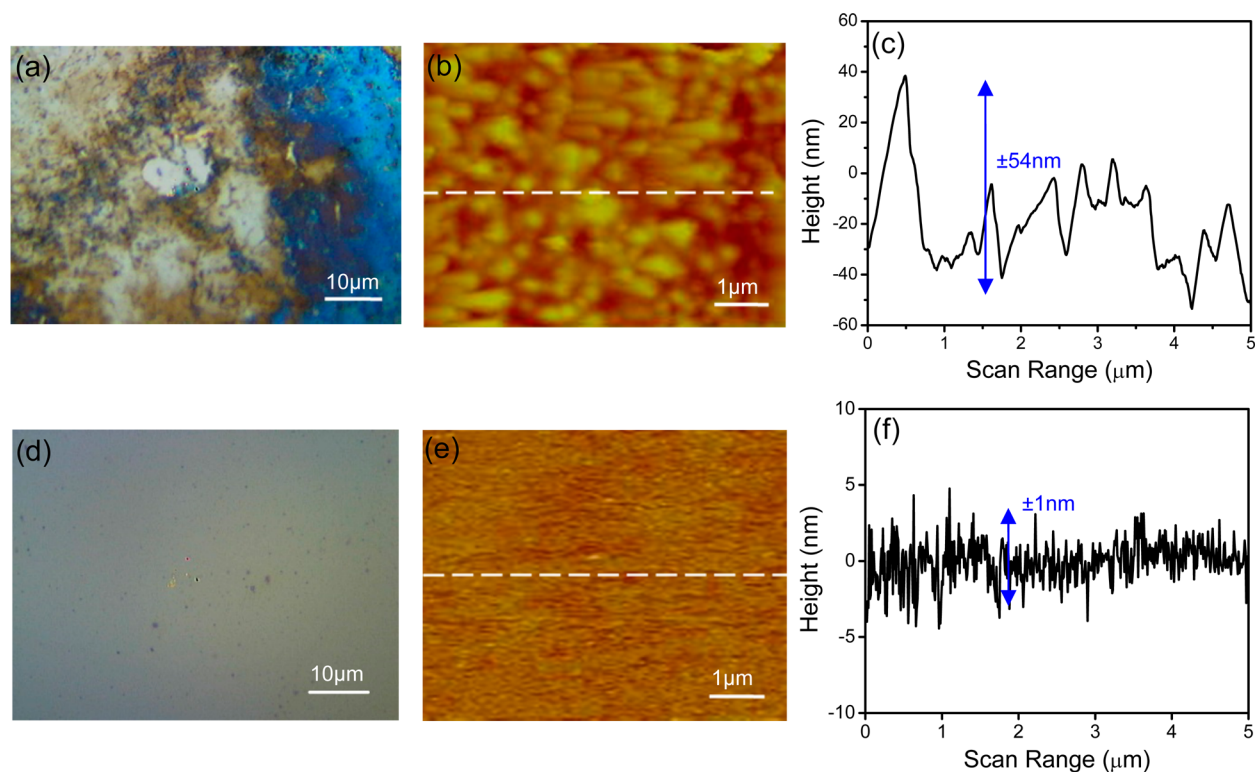


Figure 2. (a) Optical microscope image, (b) atomic force microscope image, and (c) surface topography of bare GaP surface after an 8 h reaction at -0.5 V overpotential. (d) Optical microscope image, (e) atomic force microscope image, and (f) surface topography of 5 nm TiO_2 on GaP surface after an 8 h reaction.

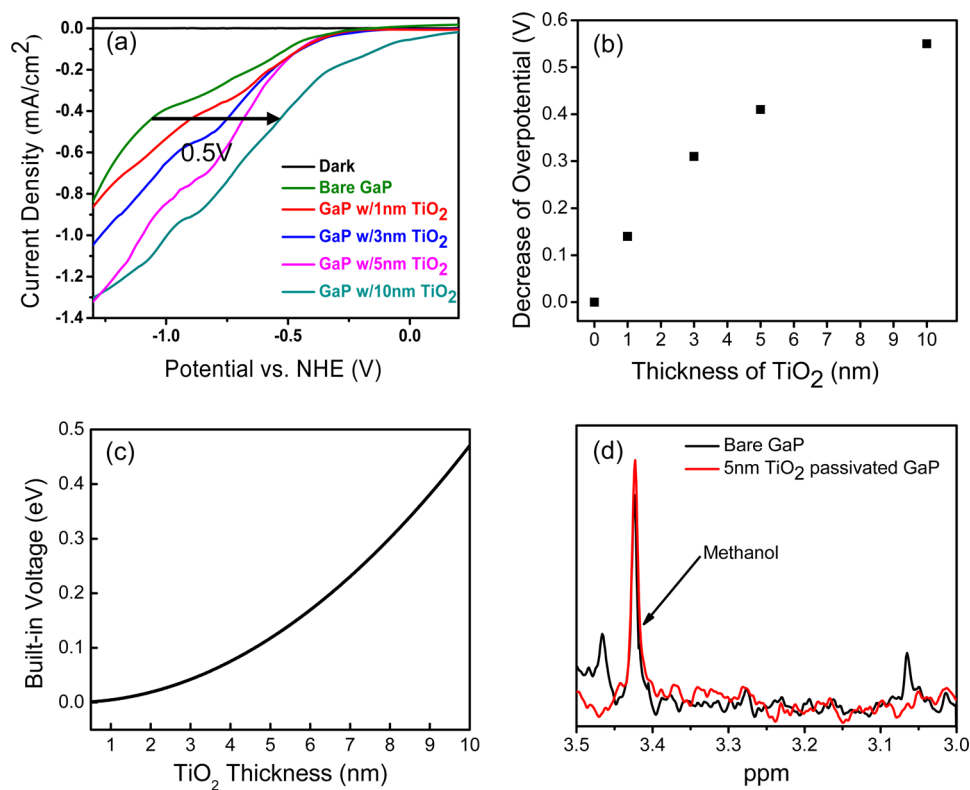


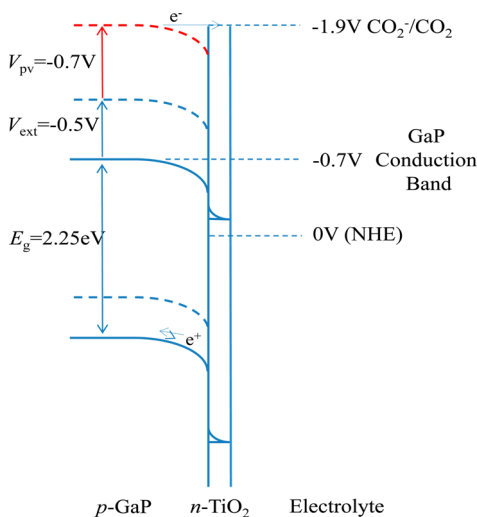
Figure 3. (a) Photocatalytic current–potential curves of GaP photocatalysts with different TiO_2 thicknesses in a 0.5 M NaCl, 10 mM pyridine solution under 532 nm wavelength laser illumination. (b) Decrease of overpotential plotted as a function of TiO_2 thickness on GaP. (c) Calculated built-in voltage plotted as a function of TiO_2 thickness. (d) NMR spectra showing methanol production using bare GaP and 5 nm TiO_2 -passivated GaP photocatalysts at an overpotential of -0.50 V.

Table 1. Shift of Onset Overpotential for Samples with Different Thicknesses of TiO₂

catalysts	shift of onset overpotential compared to bare GaP (V)
bare GaP	0
1 nm TiO ₂ @GaP	0.13
3 nm TiO ₂ @GaP	0.31
5 nm TiO ₂ @GaP	0.40
10 nm TiO ₂ @GaP	0.52

other sources of carbon in this reaction, we used isotopically labeled ¹³CO₂ as the carbon source in this reaction and observed ¹³CH₃OH in the ¹³C NMR spectrum shown in Supporting Information Figure S5.¹⁴ In addition, we repeated the experiment, purging with Ar instead of CO₂, and found no production of hydrocarbons. Therefore, we are confident that CO₂ is the only carbon source in this reaction. Previously, it was reported that a pyridine catalyst is required to drive this reaction on GaP. The pyridinium radical serves as a one-electron charge-transfer mediator, which is capable of efficiently transferring all six electrons to reduce CO₂ to methanol, thereby circumventing the high energy barrier of the one-electron reduction of CO₂ mentioned above.¹¹ However, we observe the same methanol peak in our NMR spectra without pyridine in solution (see Supporting Information Figure S2), indicating that this catalyst is not, in fact, required to drive this reaction at low overpotentials. Although CH₃OH products are observed without pyridine, the yield is one-third that of the system with pyridine, indicating that the pyridine, in fact, helps lower the energy barriers of the reaction by forming an inner-sphere-type electron-transfer system.^{11,15} Atomic force microscopy shows that the GaP/TiO₂ is photochemically stable without pyridine, as shown in Supporting Information Figure S3.

In order to understand the mechanism of this reaction, we must consider the energetics of the electrons in this photocatalytic structure. The conduction bands of GaP and TiO₂ lie slightly above NHE at -0.7 V and -0.2 V versus NHE, respectively, as plotted in Figure 4. This leaves an energy barrier of at least 1.2 V for the electrons to overcome in the reduction of CO₂. The -0.5 V externally applied overpotential

**Figure 4.** Energy band alignment of GaP and TiO₂ together with the relevant redox potentials of CO₂.

(V_{ext}) accounts for part of this required energy, and the photovoltage produced at the internal pn-junction and/or the liquid-semiconductor junction (V_{pv}) can easily account for the remaining -0.7 V, as depicted in Figure 4. From the flat-band voltage, we can obtain the open circuit voltage, as follows: $(V_{\text{oc}})_{\text{max}} = |V_{\text{fb}} - V_{\text{redox}}|$, where V_{fb} is flat-band potential and V_{redox} is the potential of the redox couple.¹⁶ From Mott–Schottky measurements, we obtained a flat-band potential of 0.4 V versus NHE, which is consistent with previous values from literature.^{3a,17} Using V_{redox} (ferricyanide/ferrocyanide) = 0.36 V, we obtain an open circuit voltage of $V_{\text{oc}} = 0.76$ V, which is large enough to cover the remaining -0.7 V depicted in Figure 4. This photovoltage is reasonable considering GaP's relatively large band gap of 2.25 eV.

These estimations assume that the electrons traverse the TiO₂ layer ballistically and do not equilibrate to the TiO₂ conduction band edge. In the diffusive case, an additional 0.5 V would be required. We believe this is one of the reasons why the TiO₂ layer must be made very thin. Several aspects of these results and their underlying mechanism are quite surprising. First, we had initially thought that the TiO₂ layer, which is insulating and has a low conduction band energy, would lower the overall photocatalytic efficiency (i.e., photocurrent), but would, at least, provide a stable, viable catalyst. Much to our surprise, the TiO₂ layer actually improved the overall photoconversion efficiency. The reasons for this are 3-fold: (1) The TiO₂ reduces nonradiative recombination of the photoexcited electron–hole pairs. (2) The electrons traverse the TiO₂ ballistically and, therefore, do not relax to the conduction band edge. (3) The formation of a pn-junction provides an additional photovoltage required to drive the reaction.

It is important to note, however, that the CO₂^{•-} reduction potential of -1.9 V versus NHE is calculated from simple thermodynamic considerations for isolated CO₂^{•-} species, and does not include the effects of the solution or catalytic surface. As a result, the energetics of the actual CO₂^{•-} intermediates can be quite different due to the presence of the aqueous solution and/or the catalytic surface. In a mechanism proposed by Anpo et al., the CO₂^{•-} intermediate is strongly bound to a proposed Ti³⁺ active site (oxygen vacancy) on the TiO₂ surface, thus lowering its energy.¹⁸ Another strategy for lowering the reaction barrier is stabilizing the CO₂^{•-} intermediate, which was recently demonstrated using an ionic liquid electrolyte cocatalyst where the cation forms a complex with the anionic intermediate.¹⁹ Two-electron processes have also been proposed by Tanaka et al., which would circumvent this first intermediate step altogether.²⁰ Although several mechanisms have been proposed in the literature, further spectroscopic studies are needed in order to verify the catalytic reaction pathway.

In conclusion, we report photocatalytic CO₂ reduction on TiO₂-passivated GaP. The TiO₂ passivation layer successfully stabilizes the GaP surface in solution, preventing it from photocorrosion. In addition, the TiO₂ passivation layer provides enhancement in the photoconversion efficiency through the passivation of surface states and the formation of a charge separating pn-region, which reduces carrier recombination and lowers the overpotential required to initiate this reaction by approximately 0.5 V. This general approach of passivating narrower band gap semiconductors with TiO₂ will enable more efficient photocatalysts to be developed and a broad range of materials to be considered for photocatalysis

that make more efficient use of the solar spectrum. We also observe CH₃OH evolution with and without pyridine catalyst, indicating that this catalysts is not, in fact, required to drive this reaction at low overpotentials.

■ ASSOCIATED CONTENT

Supporting Information

Gas chromatography data; ¹H NMR spectra of methanol; images using optical microscopy, atomic force microscopy, and surface topography, CH₃OH production plotted as a function of time; and ¹³C NMR spectrum of methanol. This material is available free of charge via the Internet at <http://pubs.acs.org>.

■ AUTHOR INFORMATION

Corresponding Author

*E-mail: scronin@usc.edu.

Notes

The authors declare no competing financial interest.

■ ACKNOWLEDGMENTS

This research was supported by ARO Award No. W911NF-14-1-0228 (J.Q.) and NSF Award No. CBET-0854118 (G.Z.).

■ REFERENCES

(1) (a) Benson, E. E.; Kubiak, C. P.; Sathrum, A. J.; Smieja, J. M. *Chem. Soc. Rev.* **2009**, *38* (1), 89–99. (b) Kumar, B.; Llorente, M.; Froehlich, J.; Dang, T.; Sathrum, A.; Kubiak, C. P. *Annu. Rev. Phys. Chem.* **2012**, *63*, 541–569. (c) Amatore, C.; Saveant, J. M. *J. Am. Chem. Soc.* **1981**, *103* (17), 5021–5023. (d) Cokoja, M.; Bruckmeier, C.; Rieger, B.; Herrmann, W. A.; Kühn, F. E. *Angew. Chem., Int. Ed.* **2011**, *50* (37), 8510–8537. (e) Finn, C.; Schnittger, S.; Yellowlees, L. J.; Love, J. B. *Chem. Commun.* **2012**, *48* (10), 1392–1399. (f) Goepfert, A.; Czaun, M.; May, R. B.; Prakash, G. K. S.; Olah, G. A.; Narayanan, S. R. *J. Am. Chem. Soc.* **2011**, *133* (50), 20164–20167. (g) Olah, G. A.; Prakash, G. K. S.; Goepfert, A. *J. Am. Chem. Soc.* **2011**, *133* (33), 12881–12898. (h) Le, M.; Ren, M.; Zhang, Z.; Sprunger, P. T.; Kurtz, R. L.; Flake, J. C. *J. Electrochem. Soc.* **2011**, *158* (5), E45–E49. (i) Bard, A. J.; Faulkner, L. R. *Electrochemical Methods: Fundamentals and Applications*, 2nd ed.; John Wiley & Sons, Inc: New York, 2001. (j) Izumi, Y. *Coord. Chem. Rev.* **2013**, *257* (1), 171–186. (k) Varghese, O. K.; Paulose, M.; LaTempa, T. J.; Grimes, C. A. *Nano Lett.* **2009**, *9* (2), 731–737.

(2) (a) Halmann, M. *Nature* **1978**, *275* (5676), 115–116. (b) Inoue, T.; Fujishima, A.; Konishi, S.; Honda, K. *Nature* **1979**, *277*, 637–638. (c) Chen, Z.; Chen, C.; Weinberg, D. R.; Kang, P.; Concepcion, J. J.; Harrison, D. P.; Brookhart, M. S.; Meyer, T. J. *Chem. Commun.* **2011**, *47* (47), 12607–12609. (d) Morris, A. J.; Meyer, G. J.; Fujita, E. *Acc. Chem. Res.* **2009**, *42* (12), 1983–1994. (e) Jacquet, O.; Frogneux, X.; Das Neves Gomes, C.; Cantat, T. *Chem. Sci.* **2013**, *4* (5), 2127–2131. (f) Costentin, C.; Drouet, S.; Robert, M.; Savéant, J.-M. *Science* **2012**, *338* (6103), 90–94. (g) Costentin, C.; Canales, J. C.; Haddou, B.; Savéant, J.-M. *J. Am. Chem. Soc.* **2013**, *135* (47), 17671–17674. (h) Canfield, D.; Frese, K. W. *J. Electrochem. Soc.* **1983**, *130* (8), 1772–1773.

(3) (a) Barton, E. E.; Rampulla, D. M.; Bocarsly, A. B. *J. Am. Chem. Soc.* **2008**, *130* (20), 6342–6344. (b) Doherty, M. D.; Grills, D. C.; Muckerman, J. T.; Polyansky, D. E.; Fujita, E. *Coord. Chem. Rev.* **2010**, *254* (21–22), 2472–2482. (c) Savéant, J.-M. *Chem. Rev.* **2008**, *108* (7), 2348–2378.

(4) Olah, G. A.; Goepfert, A.; Prakash, G. K. S. *J. Org. Chem.* **2008**, *74* (2), 487–498.

(5) Kumar, B.; Llorente, M.; Froehlich, J.; Dang, T.; Sathrum, A.; Kubiak, C. P. *Annu. Rev. Phys. Chem.* **2012**, *63*, 541–569.

(6) Taniguchi, I.; Aurian-Blajeni, B.; Bockris, J. O. M. *Electrochim. Acta* **1984**, *29* (7), 923–932.

(7) (a) Chandrasekaran, K.; Bockris, J. O. *Surf. Sci.* **1987**, *185* (3), 495–514. (b) Bockris, J. O.; Wass, J. C. *J. Electrochem. Soc.* **1989**, *136* (9), 2521–2528. (c) Bockris, J. O.; Wass, J. C. *Mater. Chem. Phys.* **1989**, *22* (3–4), 249–280.

(8) Seshadri, G.; Lin, C.; Bocarsly, A. B. *J. Electroanal. Chem.* **1994**, *372* (1–2), 145–150.

(9) Inoue, T.; Fujishima, A.; Konishi, S.; Honda, K. *Nature* **1979**, *277*, 637.

(10) Boston, D. J.; Xu, C.; Armstrong, D. W.; MacDonnell, F. M. *J. Am. Chem. Soc.* **2013**, *135* (44), 16252–16255.

(11) Barton Cole, E.; Lakkaraju, P. S.; Rampulla, D. M.; Morris, A. J.; Abelev, E.; Bocarsly, A. B. *J. Am. Chem. Soc.* **2010**, *132* (33), 11539–11551.

(12) (a) Morgan, B. J.; Watson, G. W. *J. Phys. Chem. C* **2010**, *114* (5), 2321–2328. (b) Qiu, J.; Zeng, G.; Pavaskar, P.; Li, Z.; Cronin, S. B. *Phys. Chem. Chem. Phys.* **2014**, *16* (7), 3115–3121.

(13) Neamen, D. A. *Semiconductor Physics and Devices*, 3rd ed.; McGraw-Hill: New York, 2003; pp 241–265.

(14) Fulmer, G. R.; Miller, A. J. M.; Sherden, N. H.; Gottlieb, H. E.; Nudelman, A.; Stoltz, B. M.; Bercaw, J. E.; Goldberg, K. I. *Organometallics* **2010**, *29* (9), 2176–2179.

(15) Yan, Y.; Zeitler, E. L.; Gu, J.; Hu, Y.; Bocarsly, A. B. *J. Am. Chem. Soc.* **2013**, *135* (38), 14020–14023.

(16) Bard, A. J.; Bocarsly, A. B.; Fan, F. R. F.; Walton, E. G.; Wrighton, M. S. *J. Am. Chem. Soc.* **1980**, *102* (11), 3671–3677.

(17) Grätzel, M. *Nature* **2001**, *414* (6861), 338–344.

(18) Anpo, M.; Yamashita, H.; Ichihashi, Y.; Ehara, S. *J. Electroanal. Chem.* **1995**, *396* (1–2), 21–26.

(19) Rosen, B. A.; Salehi-Khojin, A.; Thorson, M. R.; Zhu, W.; Whipple, D. T.; Kenis, P. J. A.; Masel, R. I. *Science* **2011**, *334* (6056), 643–644.

(20) Tanaka, K.; Miyahara, K.; Toyoshima, I. *J. Phys. Chem.* **1984**, *88* (16), 3504–3508.